Nanoscale

ROYAL SOCIETY OF CHEMISTRY

PAPER

View Article Online
View Journal | View Issue

Check for updates

Cite this: *Nanoscale*, 2024, **16**, 8417

A photo-responsive self-healing hydrogel loaded with immunoadjuvants and MoS_2 nanosheets for combating post-resection breast cancer recurrence†

Siyu Wang,[a] Zhuoping Qian,[a] Huaxin Xiao,[a] Guangwen Yang,[b] Ziyi Zhu,[a] Yubin Gu,[a] Junjie Song,[a] Xin Zhang,[a] Xinxuan Huang,[a] Lixing Weng,[a] Yu Gao, *[a] Wenjing Yang *[a] and Lianhui Wang *[a]

Tumor recurrence after surgical resection remains a significant challenge in breast cancer treatment. Immune checkpoint blockade therapy, as a promising alternative therapy, faces limitations in combating tumor recurrence due to the low immune response rate. In this study, we developed an implantable photo-responsive self-healing hydrogel loaded with MoS_2 nanosheets and the immunoadjuvant R837 (PVA-MoS_2-R837, PMR hydrogel) for *in situ* generation of tumor-associated antigens at the post-surgical site of the primary tumor, enabling sustained and effective activation of the immune response. This PMR hydrogel exhibited potential for near-infrared (NIR) light response, tissue adhesion, self-healing, and sustained adjuvant release. When implanted at the site after tumor resection, NIR irradiation triggered a photothermal effect, resulting in the ablation of residual cancer cells. The *in situ*-generated tumor-associated antigens promoted dendritic cell (DC) maturation. In a mouse model, PMR hydrogel-mediated photothermal therapy combined with immune checkpoint blockade effectively inhibited the recurrence of resected tumors, providing new insights for combating post-resection breast cancer recurrence.

Received 25th January 2024,
Accepted 16th March 2024

DOI: 10.1039/d4nr00372a

rsc.li/nanoscale

Published on 09 Dzivamisoko 2024. Downloaded on 2026-05-12 14:06:09.

Introduction

The recurrence of tumors following surgical resection, which is significantly associated with adverse clinical outcomes and poor overall survival, remains a major challenge in the treatment of breast cancer.[1–3] Recently, immunotherapy employing immune-checkpoint blockade has been shown to prevent tumor recurrence after surgery by blocking immune checkpoint pathways.[4–7] However, the sustained clinical response rate from patients who receive immunotherapy tends to be relatively modest (usually 10–30%) after systemic administration, particularly after surgical resection.[8] This is attributed to the development of multiple resistance pathways in the molecular, cellular and tumor microenvironments.[9,10] Hence, a novel strategy to enhance the response of immunotherapy for combating post-resection breast cancer recurrence is highly desirable.

An alternative approach involves the utilization of cancer vaccines to generate tumor-associated antigens.[11] This is achieved by implementing specific strategies with the assistance of immunoadjuvants, such as toll-like-receptor-7 (TLR-7) agonist R837, to activate dendritic cell (DC) maturation, thereby inducing potent anti-tumor immune responses.[12–15] Photothermal therapy (PTT) has been shown to inhibit not only tumor growth, but also the generation of anti-tumor immunological effects by producing tumor-associated antigens from the ablated residues of tumor cells.[16–18] The photothermal ablation of tumors may induce vaccine-like functions, enhancing immune responses to combat cancer recurrence. Consequently, combining PTT with an immune checkpoint blockade strategy has the potential to maximize the benefits of cancer immunotherapy against cancer recurrence.

An optimal strategy for improving the treatment of cancer recurrence involves the use of locally implanted biodegradable materials loaded with pharmaceuticals and external stimuli.[19–22] For example, photo-responsive self-healing hydrogels have emerged as promising candidates for the treatment of cancer.[23–25] Beyond inheriting the advantages of conven-

[a]*State Key Laboratory for Organic Electronics and Information Displays & Jiangsu Key Laboratory for Biosensors, Institute of Advanced Materials (IAM), Jiangsu National Synergistic Innovation Center for Advanced Materials (SICAM), Nanjing University of Posts & Telecommunications, Nanjing 210023, China.*
E-mail: iamygao@njupt.edu.cn, iamwjyang@njupt.edu.cn, iamlhwang@njupt.edu.cn
[b]*Nanjing Stomatological Hospital, Affiliated Hospital of Medical School, Nanjing University, Nanjing, Jiangsu 210008, China*

† Electronic supplementary information (ESI) available. See DOI: https://doi.org/10.1039/d4nr00372a

Published on 09 Dzivamisoko 2024. Downloaded on 2026-05-12 14:06:09.

tional hydrogels, they introduce an on-demand healing process through the remote manipulation of light irradiation.[26] Once the adjuvant-loaded self-healing hydrogel is implanted at the surgical site, it can self-repair under external light stimulation. This remarkable ability not only enables sustained adjuvant release without rupture of the implanted hydrogel, but also facilitates the adhesion of the hydrogel to the irregular surface of the tissue at the post-surgical site. To achieve photo-response, photothermal conversion agents have been widely applied in developing self-healing hydrogels. MoS_2 nanosheets, as excellent near-infrared (NIR) photothermal conversion agents, can induce high temperatures and contribute to not only the ablation of residual tumors but also a rapid healing process when incorporated into polyvinyl alcohol (PVA) hydrogels under NIR irradiation.[27,28]

Inspired by these findings, we developed an NIR-responsive self-healing hydrogel in combination with checkpoint blockade for inhibiting breast cancer recurrence. Self-healing PVA hydrogels encapsulating MoS_2 nanosheets and imiquimod R837 (PVA-MoS_2-R837, PMR hydrogel) were constructed using a simple freeze–thaw method (Fig. 1a). The chemically modified MoS_2 nanosheets were surface-functionalized with DL-dithiothreitol (DTT) through the coordination bonding between the defects in the nanosheets and the thiol groups in DTT. Then, DTT-modified MoS_2 nanosheets were incorporated into the PVA hydrogel through the hydrogen bonds between the hydroxyl groups in DTT and PVA to produce a hybrid hydrogel, while R837 was encapsulated in the microstructure of the hydrogel. The resulting PMR hydrogel exhibited excellent tissue adhesion, favorable photothermal properties, and notable self-healing capabilities. Upon implantation at the surgical site following primary tumor resection, the PMR hydrogel demonstrated NIR response, facilitating the localized ablation of residual cancer cells and the simultaneous generation of tumor-associated antigens. The tumor-associated antigens generated in conjunction with R837 released from the PMR hydrogel induced strong immunological responses, promoting DC maturation. With the help of an immune checkpoint blockade PD-L1 antibody (aPDL1), combination therapy effectively inhibited the recurrence of post-resection breast tumors in a mouse model (Fig. 1b).

Results and discussion

Preparation and characterization of the PMR hydrogel

To incorporate MoS_2 nanosheets into the PVA hydrogel, single-layer nanosheets were prepared and surface-modified with the thiol-containing ligand molecule DTT. The obtained DTT-modified MoS_2 nanosheets are shown in Fig. 2a and exhibit a consistent sheet-like morphology with no apparent holes or cracks. Subsequently, the PMR hydrogel was formed after the incorporation of DTT-modified MoS_2 and R837 into the PVA hydrogel. The color of the PMR hydrogel indicated a transition from white and transparent to black with the addition of MoS_2 and R837 to the PVA hydrogel (ESI Fig. 1†). As shown in Fig. 2b, the inner microstructures of the PVA hydrogels revealed a honeycomb-like porous network structure. Upon the addition of DTT-modified MoS_2, the PMR hydrogel developed a denser inner microstructure than the PVA hydrogel, which is attributed to the hydrogen bonding interactions between the hydroxyl groups in DTT and PVA (Fig. 2c). Next, we evaluated the self-healing performance of the PMR hydrogel under NIR irradiation. As shown in Fig. 2d, two pieces of the PMR hydrogel were rapidly healed upon exposure to 808 nm NIR irradiation and remained intact without breaking under moderate transverse tension. These findings suggested the excellent self-healing ability of the PMR hydrogel under NIR irradiation, reducing the potential risk of implant rupture within the body. The increased temperature at the damaged site might enhance the mobility of PVA chains and facilitate the reconstruction of hydrogen bonds, resulting in localized self-healing in the hydrogel.

An ideal hydrogel implant for post-surgical cancer therapy should be remoldable to match the irregular tissue surface of the resection site.[29] Adhesion to the surrounding tissue may prevent the movement of the implanted hydrogel, resulting in localized and efficient delivery of adjuvant to the resection site. Therefore, we first investigated the remoldability of the PMR hydrogel under NIR irradiation. As shown in Fig. 2e and f, the PMR hydrogel exhibited excellent remoldability after exposure to NIR irradiation and subsequent re-freezing/thawing in different molds or containers. Next, after NIR irradiation, the PMR hydrogel adhered tightly to various tissues of mice, including the heart, liver, spleen, lungs, and kidneys (Fig. 2g). The robust adhesion of the PMR hydrogel to various tissues might be attributed to the formation of hydrogen bonds between the hydrogel and tissues.[30] To further validate the *in vivo* applicability of the PMR hydrogel post-resection, we subcutaneously implanted the disk-shaped PMR hydrogel into the mice. Histological analysis showed close adhesion between the subcutaneous tissue and the PMR hydrogel by NIR treatment (ESI Fig. 2†). However, the PMR hydrogel did not match the surface of the subcutaneous tissue, resulting in an observable gap between the implant and the tissue. These results indicated the excellent remoldability and tissue adhesion of the self-healing PMR hydrogel, making it suitable for use as an adjuvant delivery platform for the post-surgical site.

Photothermal performance of the PMR hydrogel

Based on the excellent photothermal ability of the MoS_2 nanosheets, we conducted an *in vitro* study to examine the photothermal performance of the PMR hydrogel (Fig. 3a). The results revealed that the temperature increase of the PMR hydrogel with MoS_2 (1 mg ml^{-1}) was dependent on the laser power (Fig. 3b). Specifically, the temperature of the PMR hydrogel increased to approximately 44 °C, 55 °C and 60 °C at a laser power of 0.5 W cm^{-2}, 0.75 W cm^{-2}, and 1 W cm^{-2}, respectively (Fig. 3c). As the optimal temperature for the *in vivo* immune response is 43–45 °C,[6,31,32] a laser power of 0.5 W cm^{-2} was selected for *in vitro* and *in vivo* studies. Under a con-

 This journal is © The Royal Society of Chemistry 2024

Published on 09 Dzivamisoko 2024. Downloaded on 2026-05-12 14:06:09.

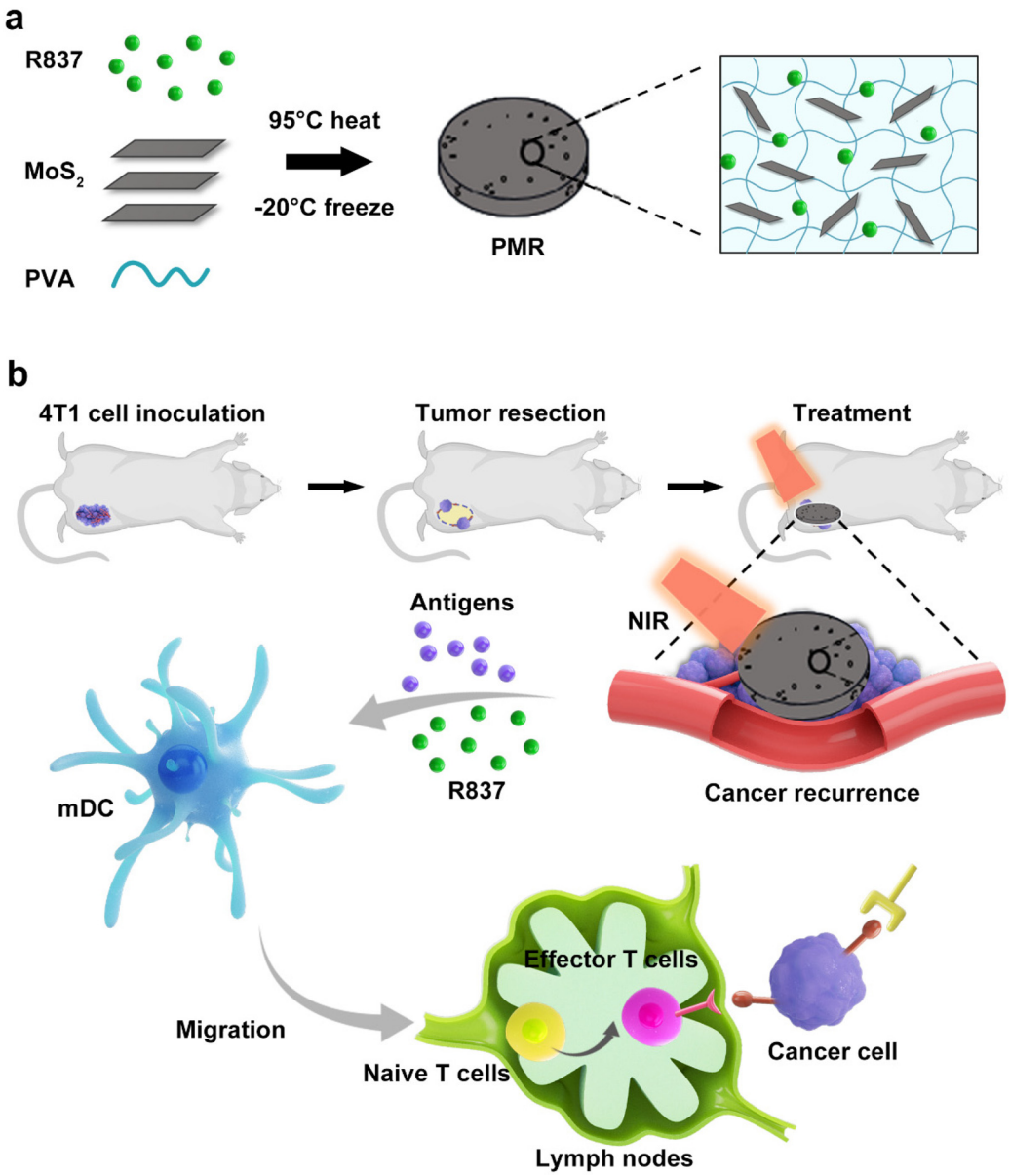

Fig. 1 (a) Schematic illustration of the preparation of the photo-responsive self-healing PMR hydrogel *via* the freeze–thaw method. (b) Schematic illustration of tumor recurrence inhibition by PMR-based PTT in combination with the immune checkpoint blockade.

stant laser power (0.5 W cm^{-2}), the temperature of the PMR hydrogel increased similarly to that observed in the PM hydrogel, suggesting that the incorporation of the R837 did not compromise the photo-response of MoS_2 nanosheets (Fig. 3d and e). In the absence of MoS_2 nanosheets, a slight temperature increase was observed in the PVA hydrogels following NIR irradiation, which was similar to the PBS control group. Moreover, periodic laser irradiation on/off resulted in repeatable temperature changes, indicating the good photothermal stability of the PMR hydrogel (Fig. 3f).

Next, we investigated the photothermal performance of the PMR hydrogel *in vivo*. The PVA-MoS_2 hydrogel (PM hydrogel without R837), PVA hydrogel (without R837 and MoS_2 nanosheets), and PBS were used as controls. The PMR hydrogels were subcutaneously implanted into mice and subjected to NIR irradiation for 5 minutes. As shown in ESI Fig. 3,† the temperature of both the PMR hydrogel and the PM hydrogel quickly reached 45 °C within 5 minutes, which was significantly greater than that of the implanted PVA hydrogel and the subcutaneously injected PBS, suggesting their potential for efficient photothermal therapy *in vivo*.

In vitro and *in vivo* adjuvant release

It has been reported that R837 can promote DC maturation *in vivo*.[16] We set to study the release behavior of R837 from the PMR hydrogel platform. As shown in Fig. 4a, the burst release

Published on 09 Dzivamisoko 2024. Downloaded on 2026-05-12 14:06:09.

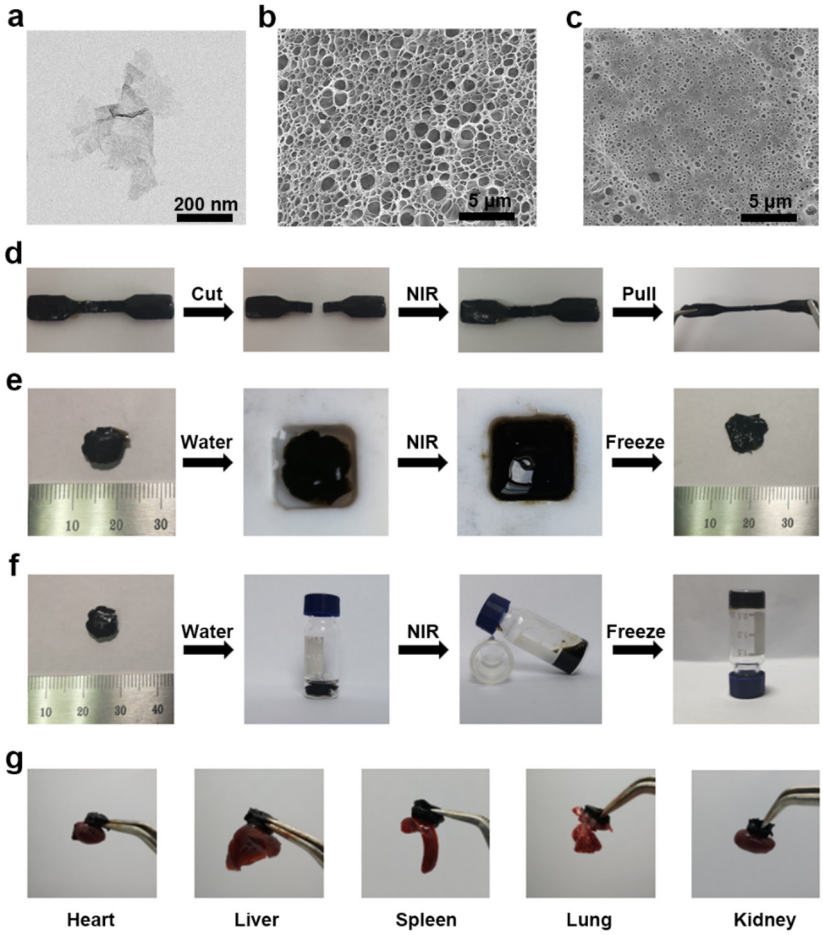

Fig. 2 Characterization of the photo-responsive self-healing PMR hydrogel. (a) Representative TEM images of DTT-modified MoS_2 nanosheets. Scale bar: 200 nm. (b) Representative SEM images of the PVA hydrogel. Scale bar: 5 μm. (c) Representative SEM images of the PMR hydrogel. Scale bar: 5 μm. (d) Photographs of the self-healing process of the PMR hydrogels after NIR irradiation (808 nm, 0.5 W cm^{-2}) for 5 minutes. (e) Photographs of the remoldability process of a disk-shaped PMR hydrogel after NIR irradiation (808 nm, 1 W cm^{-2}, 5 minutes) and freezing in a square mold. (f) Photographs of the remoldability process of the PMR hydrogels after NIR irradiation (808 nm, 1 W cm^{-2}, 5 minutes) and freezing in a glass vial. (g) Photographs of the adhesions between the PMR hydrogel and *ex vivo* mouse primary organs, including the heart, liver, spleen, lung, and kidney, after NIR irradiation (808 nm, 1 W cm^{-2}, 5 minutes).

was observed in the PVA-R837 hydrogel (PR hydrogel without MoS_2 nanosheets), PMR hydrogel (without NIR), and PMR hydrogel with NIR irradiation, accounting for 52.2%, 40.04% and 43.9% of the R837 released after 24 h, respectively. Subsequently, the release rate of R837 significantly decreased in all the groups, reaching a plateau after 6 days. The released content from the PMR hydrogel (without NIR) was lower than that from the PR hydrogel, which might be attributed to the interaction between the thiol functional groups of MoS_2 and the hydroxyl groups of PVA. This interaction limits the effect of the swelling behavior of the hydrogel, consequently reducing the adjuvant diffusion and release. In addition, the NIR irradiation did not impact the release behavior of R837 from the PMR hydrogel, as similar release profiles were observed for the PMR hydrogel with or without NIR irradiation.

In vivo drug release was also studied by implanting the hydrogel into the subcutaneous area of mice. To monitor the adjuvant release, R837 was replaced by a fluorescent dye Cy5.5 to form the PVA-Cy5.5 hydrogel (PC hydrogel without MoS_2 nanosheets) and PVA-MoS_2-Cy5.5 hydrogel (PMC hydrogel), and the fluorescence intensity of Cy5.5 was monitored and quantified *in vivo*. As shown in Fig. 4b and c, the fluorescence intensity gradually decreased in both the implanted PC hydrogel and the PMC hydrogel. The fluorescence intensities of the PC hydrogel and PMC hydrogel decreased to 65.4% and 69.9% after 24 hours, and reached a plateau after 10 days, respectively. Compared to the rapid clearance of subcutaneously injected adjuvants,[19,33] the sustained adjuvant release in 10 days achieved by the PMC hydrogel might induce a prolonged immune response, thereby efficiently suppressing tumor recurrence over a relatively long period.

In vitro DC maturation assay

The *in vitro* biocompatibility of the PMR hydrogel was first assessed by culturing the PMR hydrogel with 4T1 cells. After 24 hours, the cell viability for all treatments remained above

 This journal is © The Royal Society of Chemistry 2024

Published on 09 Dzivamisoko 2024. Downloaded on 2026-05-12 14:06:09.

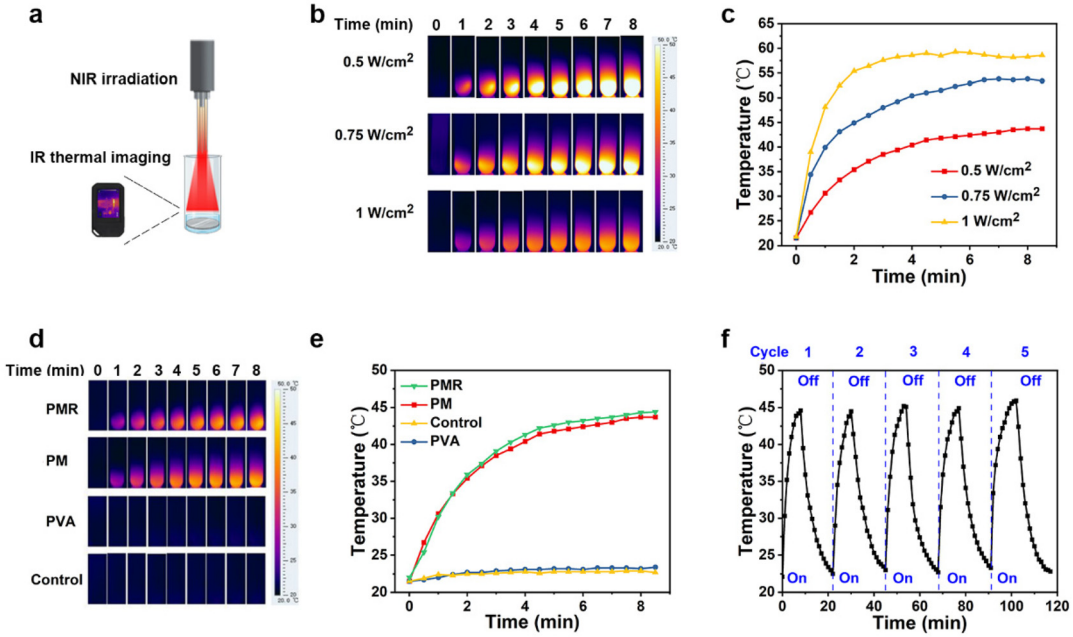

Fig. 3 Photothermal performance of the photo-responsive self-healing PMR hydrogel. (a) Schematic illustration of the PMR hydrogel for infrared radiation (IR) imaging. (b) Representative IR thermal images of the PMR hydrogel at different 808 nm NIR laser irradiation powers. (c) Temperature elevation curves of the PMR hydrogel suspension at different NIR laser irradiation powers. (d) Representative IR images of the PMR hydrogel, PM hydrogel, and PVA hydrogel at 0.5 W cm^{-2} NIR irradiation. (e) Temperature elevation curves of the PMR hydrogel, PM hydrogel, and PVA hydrogel at 0.5 W cm^{-2} NIR irradiation. (f) Photothermal stability of the PMR hydrogel during the circles of heating and cooling cycles at 0.5 W cm^{-2} NIR irradiation.

90% in comparison to that of the control group. However, following irradiation with an 808 nm NIR laser at a power of 1.5 W cm^{-2} or 1 W cm^{-2} for 5 minutes, the inhibition efficiency of the cocultured 4T1 cells after 24 h was determined as 80% and 60%, respectively (ESI Fig. 4†). The power of 1 W cm^{-2} was applied in subsequent *in vitro* photothermal-immune combination therapy, as the temperature reached 45 °C, indicating that a gentle photothermal effect is involved in promoting the formation of a favourable immune microenvironment.

DCs, crucial antigen-presenting cells (APCs) in antitumor immunity, play vital roles in the response to antigens.[34] Hyperthermia and R837 have been reported to promote DC maturation *in vivo*. To investigate whether the R837-loaded PMR hydrogel combined with PTT can promote DC maturation, transwell assays were established for the following studies. First, the DCs isolated from BALB/c mice were cultured with the PMR hydrogel (inserted well) (Fig. 5a). Flow cytometry was employed to analyze the presence of co-stimulatory molecules CD80 and CD86 (the marker of DC maturation). The results showed an increased percentage of CD80 and CD86 in the free R837 ($CD11c^+CD80^+$: 45.8%; $CD11c^+CD86^+$: 52.4%) and PMR hydrogel ($CD11c^+CD80^+$: 36.2%, $CD11c^+CD86^+$: 37.9%) groups in comparison to those in the PBS ($CD11c^+CD80^+$: 24.9%, $CD11c^+CD86^+$: 24.5%) and PM group ($CD11c^+CD80^+$: 28.3%, $CD11c^+CD86^+$: 29.8%) (Fig. 5b). Although the PMR hydrogel significantly induced DC maturation, the percentage of mature DCs was lower than that of the free R837 group, which can be attributed to the partial release of R837 from the PMR hydrogel. DC maturation led to increased secretion of cytokines. The levels of Interleukin 10 (IL-10) and tumor necrosis factor (TNF)-α in the supernatant were significantly greater in the free R837 and PMR hydrogel groups than those in the PBS and PM groups. These results further indicated that the PMR hydrogel was able to activate DCs *in vitro* (Fig. 5c).

Apoptotic tumor cells can release inflammatory factors and tumor-associated antigens to activate DCs, present antigens to T cells, and induce robust antitumor immune responses. After the incubation of 4T1 cells with the PMR hydrogel followed by laser irradiation, the cell media supernatant containing apoptotic 4T1 cells was used to stimulate immature DCs for 24 hours. CD80 and CD86 expression on DCs was characterized by flow cytometry (Fig. 5d). The results showed increased percentages of $CD11c^+CD80^+$ and $CD11c^+CD86^+$ cells in both the 4T1 treated and PMR (without NIR irradiation) treated groups compared to those in the PBS treated group. The generated various tumor-associated antigens from the normal 4T1 cell might be attributed to the maturation of DCs, and the released R837 from the PMR hydrogel also activated the DC maturation. Notably, the percentages of $CD11c^+CD80^+$ and $CD11c^+CD86^+$ cells were substantially higher in the PM (with NIR irradiation) and PMR (with NIR irradiation) groups than those in the 4T1 treated and PMR (without NIR irradiation) treated groups (Fig. 5e). These findings suggested the presence of a substantially greater amount of tumor-associated antigens induced by the apoptotic 4T1 cells under NIR irradiation than

Published on 09 Dzivamisoko 2024. Downloaded on 2026-05-12 14:06:09.

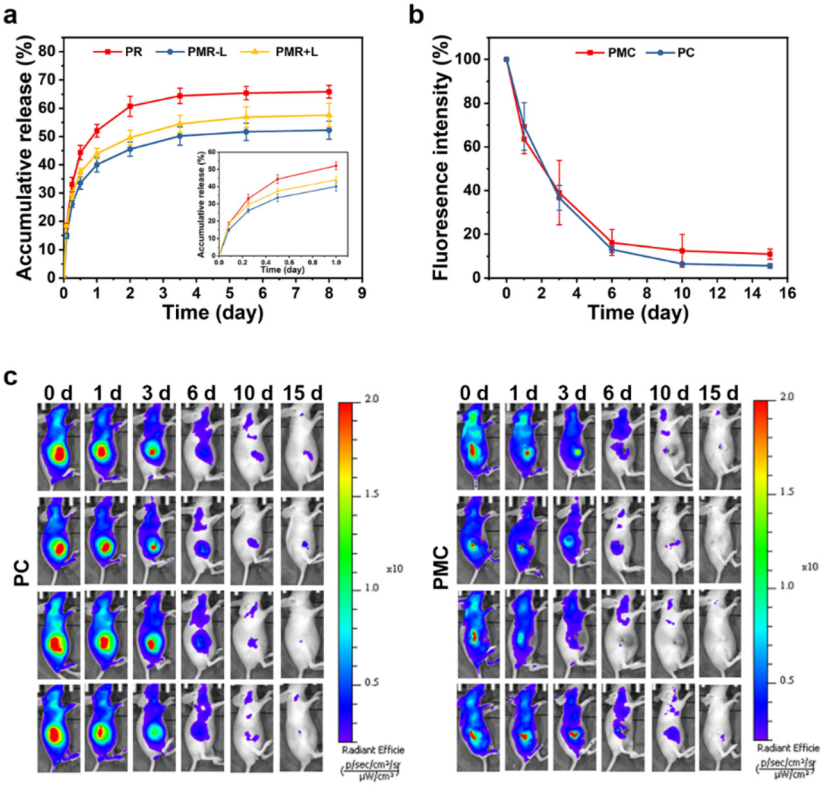

Fig. 4 The drug release profile from the photo-responsive self-healing hydrogel. (a) Cumulative R837 release from the PR hydrogel and PMR hydrogel (encapsulating R837) with or without NIR irradiation (808 nm, 0.5 W cm^{-2}, 5 minutes). Inset: cumulative R837 release profile over 1 day, n = 3. (b) Quantification of the fluorescence intensities of the subcutaneously implanted Cy5.5 loaded PMC hydrogel and the Cy5.5 loaded PC hydrogel (encapsulating Cy5.5), n = 3. (c) Representative fluorescence images of the subcutaneously implanted Cy5.5 loaded PC hydrogel and Cy5.5 loaded PMC hydrogel (encapsulating Cy5.5) at different time points.

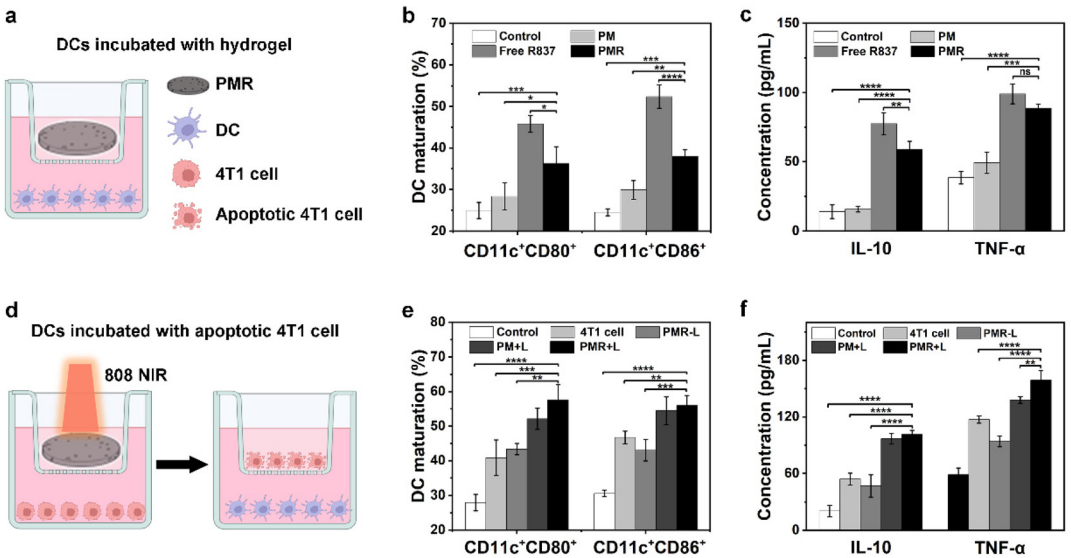

Fig. 5 The PMR hydrogel enhances DC maturation *in vitro*. (a) Schematic illustration of PMR hydrogel incubated with DCs in a transwell assay. (b) Quantification of CD80 and CD86 expression levels in DCs after different treatments, n = 3. (c) Quantification of cytokine levels of IL-10 and TNF-α in the supernatant after different treatments, n = 3. (d) Schematic illustration of the PMR hydrogel in combination with NIR irradiation (808 nm, 1 W cm^{-2}, 5 minutes) enhanced DC maturation. (e) Quantification of CD80 and CD86 expression levels in DCs after different treatments, n = 3. (f) Quantification of cytokine levels of IL-10 and TNF-α in the supernatant after different treatments, n = 3. All data were expressed as the mean ± SD. Statistical significance was calculated by one-way ANOVA with the Tukey *post hoc* test. ns, $P > 0.05$, $^{*}P < 0.05$, $^{**}P < 0.01$, $^{***}P < 0.001$, $^{****}P < 0.0001$.

This journal is © The Royal Society of Chemistry 2024

Published on 09 Dzivamisoko 2024. Downloaded on 2026-05-12 14:06:09.

in the other groups, thereby further promoting the maturation of DCs. Similarly, both the IL-10 and TNF-α levels in the PM (with NIR irradiation) and PMR (with NIR irradiation) groups were higher than those in the other groups (Fig. 5f).

PMR hydrogel-mediated combination therapy improves the therapeutic efficacy against tumor recurrence

To evaluate the *in vivo* effectiveness against tumor recurrence by PMR hydrogel-mediated PTT combined with aPDL1 therapy, a mouse model with a post-surgical 4T1 xenograft tumor was used. Luciferase-labeled 4T1 cells were subcutaneously administered to the BALB/c mice. The mice were randomly divided into four groups and 95% of each tumor was surgically removed. Then the mice were subsequently subjected to various treatments, and the effectiveness of the various treatments in preventing tumor recurrence was evaluated by monitoring the bioluminescence intensity over 22 days (Fig. 6a). As shown in Fig. 6b and c, residual tumors in all groups began to grow at 8 days post-treatment. Both the PBS-treated group and the PMR-treated group (without NIR) showed gradual tumor growth, resulting in tumor regrowth within 22 days. In contrast, the PMR combined with the aPDL1 treated group showed slight inhibition of tumor growth, possibly due to the immune effects of aPDL1. Remarkably, the combination of PMR-mediated PTT (with NIR irradiation) and aPDL1 treatment led to significant inhibition of the bioluminescence intensity, indicating the efficacy of the combined treatment in suppressing tumor recurrence. After 22 days, the tumor tissues were collected and weighed, and the results in tumor mass were consistent with the results in bioluminescence imaging (Fig. 6d). The body weight of each group was recorded every other day during the treatments, and no substantial change in the body weight was observed for each group throughout the observation period (ESI Fig. 5†). These results indicated that the anti-recurrence efficiency by the combination of PMR hydrogel-mediated PTT and aPDL1 treatment was higher than that of the PMR + aPDL1 or PMR treatment groups.

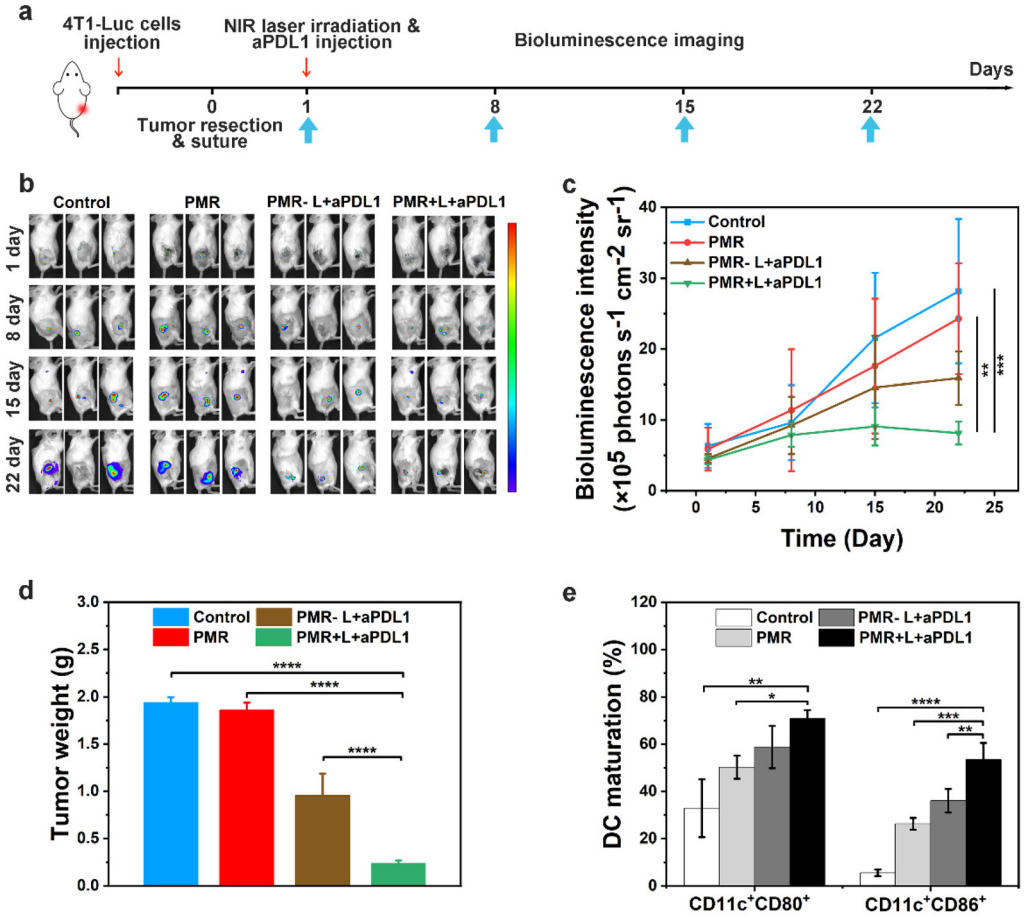

Fig. 6 The PMR hydrogel meditated PTT combined with aPDL1 inhibits tumor recurrence in a post-surgical mouse model bearing a 4T1 xenograft tumor. (a) Schematic illustration of the PMR hydrogel meditated PTT combined with aPDL1 treatment schedule. NIR irradiation: 808 nm at 1 W cm^{-2} for 5 minutes. (b) Representative bioluminescence images of the mice after various treatments. (c) Quantification of the bioluminescence intensities in b, n = 5. (d) Weights of excised tumors after different treatments, n = 5. (e) Quantification of DC maturation after various treatments, n = 5. All data were expressed as the mean ± SD. Statistical significance was calculated by one-way ANOVA with the Tukey *post hoc* test. *P < 0.05, **P < 0.01, ***P < 0.001, ****P < 0.0001.

Published on 09 Dzivamisoko 2024. Downloaded on 2026-05-12 14:06:09.

Previously, *in vitro* results confirmed that PMR hydrogel-mediated PTT promotes DC maturation by the generated tumor-associated antigens and released R837. To validate the *in vivo* therapeutic mechanism of the combination therapy, tumor-draining lymph nodes from the mice subjected to different treatments were collected for assessment using flow cytometry. The PMR-mediated PTT combined with aPDL1 achieved the highest DC maturation ($CD11c^+CD80^+$: 70.9%, $CD11c^+CD86^+$: 53.4%), which was much higher than those observed in the groups treated with PMR alone ($CD11c^+CD80^+$: 50.2%, $CD11c^+CD86^+$: 26.2%) or PMR + aPDL1 ($CD11c^+CD80^+$: 58.8%, $CD11c^+CD86^+$: 36.0%) (Fig. 6e). The results suggested that the combination therapy could induce enhanced DC maturation, leading to the improved therapeutic efficacy against tumor recurrence. Finally, histological analysis was conducted on the main organs extracted from the mice, revealing no apparent organ damage or inflammatory lesions in any of the organ sections following the treatment (ESI Fig. 6†).

Conclusion

In conclusion, we developed a photo-responsive self-healing PMR hydrogel loaded with MoS_2 nanosheets and R837, which effectively inhibited tumor recurrence after breast tumors were resected. The PMR hydrogel exhibited excellent tissue adhesion, self-healing capability, and remoldability performance for local implantation *in vivo*. Additionally, the PMR hydrogel achieved not only efficient photothermal conversion for killing cancer cells, but also sustained the release of the immune adjuvant R837, thereby promoting the maturation of DCs in a synergistic way. Considering the challenges of recurrence of post-surgical breast tumors, our strategy provides new insights for addressing tumor recurrence in future clinical applications.

Experimental

Materials, cells, and animals

MoS_2 powder (<2 μm, 99%), DL-dithiothreitol (DTT, 99%), and poly(vinyl alcohol) (PVA) were purchased from Sigma-Aldrich. *n*-Butyllithium (*n*-BuLi, 2.4 M hexane solution) was obtained from Alfa Aesar. Dimethyl sulfoxide (DMSO, >99.9%), (4,5-dimethylthiazol-2-yl)-2,5-diphenyl tetrazolium bromide (MTT) and luciferase-tagged 4T1 breast cancer cells were obtained from KeyGen Biotech Co. Ltd. Imiquimod was purchased from Solarbio. The antibodies used in this study, including anti-CD80-PE, anti-CD86-FITC, and anti-CD11c-APC, were purchased from eBioscience. All other reagents and solvents were obtained from Sigma. BALB/c mice (6–8 weeks, female) were acquired from the Nanjing Qinglong Mountain Animal Breeding Field, and the animal experiments were approved by the Animal Ethical and Welfare Committee of Nanjing University. Bone marrow-derived dendritic cells (DCs) were differentiated from the femurs and tibias of mice using previously reported methods.

Preparation of the PMR hydrogel

The PMR hydrogels were produced through a simple freeze–thaw method. Briefly, single-layer MoS_2 nanosheets were generated using an ultrasound-assisted lithium intercalation method. These MoS_2 nanosheets were subsequently surface-modified by the thiol-containing ligand molecule DTT. R837 was first dissolved in DMSO using ultrasound at a concentration of 50 mg mL^{-1}, and then diluted to 10 mg mL^{-1} using PBS. Then, 1 mg of PVA and 0.2 mL of R837 (10 mg mL^{-1}) were introduced into 3.8 mL of the DTT-modified MoS_2 nanosheet solution. The mixture was stirred at 95 °C for 15 minutes to form a uniform solution. The resulting solution was rapidly injected into a mold and cooled at −20 °C for 1 hour. Ultimately, the PMR hydrogels were obtained after thawing at room temperature for 12 hours.

Characterization of the PMR hydrogel

The morphology of MoS_2 nanosheets was examined using a transmission electron microscope (TEM, H-7500, Hitachi, Japan). The internal microstructures of the freeze-dried state PMR hydrogels were analyzed with a scanning electron microscope (SEM, S-4800, Hitachi, Japan). In the self-healing investigation, the PMR hydrogel was prepared with a mold of a dumbbell shape. Then the PMR hydrogel was cut into two parts and the two halves were rejoined and exposed to NIR (808 nm, 0.5 W cm^{-2}) for 5 minutes. The self-healing performance was determined by using tweezers to gently pull both ends of the hydrogel, and the healing process was recorded by taking pictures after 5 minutes.

Adhesive properties of the PMR hydrogel

The prepared PMR hydrogel was placed in a square mold and a 1.5 mL vial. Subsequently, an appropriate amount of DI water was added. The samples were then exposed to 808 nm NIR light (1 W cm^{-2}) for 5 minutes with stirring during the irradiation. Following the irradiation, the samples were stored at −20 °C and frozen for 1 hour.

The main organs of the mice were collected, and they were individually adhered to the PMR hydrogel. After irradiation under 808 nm NIR (1 W cm^{-2}) for 5 minutes, the hydrogel was lifted with tweezers, and the interaction between the hydrogel and the main organs was observed.

Photothermal effects *in vitro*

The photothermal behaviors of PMR hydrogels were evaluated with an 808 nm NIR laser. Briefly, the PMR hydrogel was immersed in the water and irradiated with the different NIR laser powers (0.5 W cm^{-2}, 0.75 W cm^{-2}, 1.0 W cm^{-2}) for 8 minutes. Temperatures of the PMR hydrogel could be monitored using an infrared thermal imaging camera. Furthermore, the photothermal stability of the PMR was tested through five laser on/off cycles by irradiation with an 808 nm laser.

 This journal is © The Royal Society of Chemistry 2024

Published on 09 Dzivamisoko 2024. Downloaded on 2026-05-12 14:06:09.

Drug release profile

To study the release of R837 from the hydrogels, PM and PMR hydrogels were prepared. All the samples were seeded in a 24-well plate and each well received 1 mL of PBS. The solutions in each well were collected at specific time intervals for the assessment of released R837. To determine the effect of NIR light on R837 release, the PMR hydrogels were divided into two groups: one group without laser irradiation and another group irradiated with 808 nm NIR light at 0.5 W cm^{-2} for 5 minutes.

To study *in vivo* release profiles, R837 was replaced by Cy5.5. The PC hydrogel and PMC hydrogel containing Cy5.5 were surgically implanted into mice. Then the mice were imaged using an *in vivo* imaging system (IVIS Lumina K Series III, PerkinElmer) at specified time points.

Cell cytotoxicity

4T1 cells were seeded into transwell plates (24-well) at a density of 5×10^4 and allowed to adhere. Then, PBS, PVA hydrogel, PM hydrogel, and PMR hydrogel were added to the inner wells of the plates. After 12 hours of incubation, a laser at 808 nm with 1 W cm^{-2} was applied for 5 minutes. The cell viability was tested by the MTT assay after an additional 12 hours of incubation.[35] For the PMR hydrogel group, cell viability was also tested with the application of a laser at 1.5 W cm^{-2}.

Assessment of DC maturation *in vitro*

DCs were extracted from the bone marrow of 6-week-old BALB/c mice following an established method.[33,34] Immature DCs were counted and seeded into 24-well plates at a density of 2×10^5 cells per well at the lower chamber of the transwell. The PBS, free R837, PM hydrogel, or PMR hydrogel were placed in the upper chamber. After 24 h incubation, the DCs were washed and stained with antibodies, including anti-CD80, anti-CD86, and anti-CD11c for flow cytometry analysis. Specifically, the cells were resuspended in 100 μL of PBS and then incubated with 1 μL each of the CD11c antibody and either 1 μL CD86 or CD80 antibody. After 30 min of staining, the cells were washed twice with PBS before analysis. Supernatants of the DC culture medium were collected and analyzed by ELISA kits of TNF-α, and IL-10 according to the manufacturer's instructions.

To study the impact of the photothermal immunotherapy-based PMR hydrogel system on DC maturation, the 4T1 cancer cells were subjected to pretreatment with PBS, PM hydrogel, and PMR hydrogel for 12 hours following irradiation with an NIR laser (808 nm, 1 W cm^{-2}, 5 minutes). Additionally, residues from 4T1 cells in different groups were introduced into the DC culture using a transwell system. After 24 hours incubation, the DCs were collected and analyzed by flow cytometry following the described above. Supernatants of the DC culture medium were collected and analyzed by ELISA kits.

Inhibition of tumor recurrence *in vivo*

Luciferase-tagged 4T1 cells were subcutaneously administered to each BALB/c mouse. After the tumors reached a volume of approximately 100 mm^3, the mice were randomly divided into four groups. Subsequently, the tumors were surgically removed, and 5% of residual tumor tissue remained in the surgical bed. The resection cavities were filled with the PMR hydrogel and the wounds were sutured using sterile surgical sutures. After 24 hours, one group of mice in the PMR treatment group was irradiated with 808 nm NIR at 1 W cm^{-2} for 5 minutes, accompanied by an intraperitoneal injection of 10 μg of aPDL1. Tumor volumes were recorded every 2 days using a digital caliper and calculated according to the formula: length × width^2 × 0.5. The mice were imaged at 1, 8, 15, and 22 days after hydrogel implantation *via* an IVIS imaging system. After 3 weeks, the tumors were removed and weighed. The lymph nodes were collected to analyze $CD11c^+CD80^+$ and $CD11c^+CD86^+$ DCs by flow cytometry.

Statistical analysis

All data were expressed as means ± SD. Inter- and intragroup comparisons and analysis in each experiment were performed by one-way analysis of variance (ANOVA) using the GraphPad Prism software, and $P < 0.05$ was regarded as statistically significant.

Ethical statement

The animal experiment was approved by the Animal Ethical and Welfare Committee of Nanjing University. Mouse feeding, care protocols, and experiments strictly followed the ethical standards of animal experiments at Nanjing University (IACUC-D2102069).

Author contributions

Y. G., W. J. Y., and L. H. W. designed the study. S. Y. W., Z. P. Q., H. X. X., and G. W. Y. carried out synthesis, characterization, and all *in vitro* assays. S. Y. W., Y. B. G., J. J. S., X. Z., X. X. H., and L. X. W. performed the *ex vivo* and animal experiments. Y. G., S. W. Y., W. J. Y., and L. H. W. wrote the manuscript.

Conflicts of interest

The authors declare that they have no competing interests.

Acknowledgements

This work was supported by the Natural Science Foundation of Jiangsu Province-Major Project (BK20212012), the Natural Science Foundation of China (22277058), and the Natural Science Foundation of Jiangsu Province (BK20221331).

Published on 09 Dzivamisoko 2024. Downloaded on 2026-05-12 14:06:09.

References

1 C. Yau, M. Osdoit, M. van der Noordaa, S. Shad, J. Wei, D. de Croze, A. S. Hamy, M. Lae, F. Reyal, G. S. Sonke, T. G. Steenbruggen, M. van Seijen, J. Wesseling, M. Martin, M. Del Monte-Millan, S. Lopez-Tarruella, I. S. T. Consortium, J. C. Boughey, M. P. Goetz, T. Hoskin, R. Gould, V. Valero, S. B. Edge, J. E. Abraham, J. M. S. Bartlett, C. Caldas, J. Dunn, H. Earl, L. Hayward, L. Hiller, E. Provenzano, S. J. Sammut, J. S. Thomas, D. Cameron, A. Graham, P. Hall, L. Mackintosh, F. Fan, A. K. Godwin, K. Schwensen, P. Sharma, A. M. DeMichele, K. Cole, L. Pusztai, M. O. Kim, L. J. van 't Veer, L. J. Esserman and W. F. Symmans, *Lancet Oncol.*, 2022, **23**, 149–160.

2 G. W. Sledge, E. P. Mamounas, G. N. Hortobagyi, H. J. Burstein, P. J. Goodwin and A. C. Wolff, *J. Clin. Oncol.*, 2014, **32**, 1979–1986.

3 D. A. Mahvi, R. Liu, M. W. Grinstaff, Y. L. Colson and C. P. Raut, *CA Cancer J. Clin.*, 2018, **68**, 488–505.

4 A. Ribas and J. D. Wolchok, *Science*, 2018, **359**, 1350–1355.

5 S. L. Topalian, P. M. Forde, L. A. Emens, M. Yarchoan, K. N. Smith and D. M. Pardoll, *Cancer Cell*, 2023, **41**, 1551–1566.

6 Y. Gao, X. Chen, B. Wang, S. Wang, J. Wang, L. Ren, W. K. Jin, H. Han and L. Wang, *ACS Appl. Bio Mater.*, 2023, **6**, 257–266.

7 Z. Li, Y. Ding, J. Liu, J. Wang, F. Mo, Y. Wang, T. J. Chen-Mayfield, P. M. Sondel, S. Hong and Q. Hu, *Nat. Commun.*, 2022, **13**, 1845.

8 Q. Hu, H. Li, E. Archibong, Q. Chen, H. Ruan, S. Ahn, E. Dukhovlinova, Y. Kang, D. Wen, G. Dotti and Z. Gu, *Nat. Biomed. Eng.*, 2021, **5**, 1038–1047.

9 M. R. Junttila and F. J. de Sauvage, *Nature*, 2013, **501**, 346–354.

10 J. Zhang, C. Chen, A. Li, W. Jing, P. Sun, X. Huang, Y. Liu, S. Zhang, W. Du, R. Zhang, Y. Liu, A. Gong, J. Wu and X. Jiang, *Nat. Nanotechnol.*, 2021, **16**, 538–548.

11 M. E. Aikins, C. Xu and J. J. Moon, *Acc. Chem. Res.*, 2020, **53**, 2094–2105.

12 L. Wang, Y. He, T. He, G. Liu, C. Lin, K. Li, L. Lu and K. Cai, *Biomaterials*, 2020, **255**, 120208.

13 H. Dong, Q. Li, Y. Zhang, M. Ding, Z. Teng and Y. Mou, *Adv. Sci.*, 2023, **10**, e2301339.

14 Q. Li, Z. Teng, J. Tao, W. Shi, G. Yang, Y. Zhang, X. Su, L. Chen, W. Xiu, L. Yuwen, H. Dong and Y. Mou, *Small*, 2022, **18**, e2201108.

15 R. Qu, D. He, M. Wu, H. Li, S. Liu, J. Jiang, X. Wang, R. Li, S. Wang, X. Jiang and X. Zhen, *Nano Lett.*, 2023, **23**, 4216–4225.

16 Q. Chen, L. Xu, C. Liang, C. Wang, R. Peng and Z. Liu, *Nat. Commun.*, 2016, **7**, 13193.

17 Y. Yin, S. Wang, D. Hu, J. Cai, F. Chen, B. Wang and Y. Gao, *J. Visualized Exp.*, 2020, **159**, e61208.

18 W. Shao, F. Zhao, J. Xue and L. Huang, *BMEMat*, 2023, **1**, e12009.

19 Y. Gao, J. Wang, H. Han, H. Xiao, W. K. Jin, S. Wang, S. Shao, Z. Wang, W. Yang, L. Wang and L. Weng, *Nanoscale*, 2021, **13**, 14417–14425.

20 L. L. Bu, J. Yan, Z. Wang, H. Ruan, Q. Chen, V. Gunadhi, R. B. Bell and Z. Gu, *Biomaterials*, 2019, **219**, 119182.

21 S. Wang, X. Guo, W. Xiu, Y. Liu, L. Ren, H. Xiao, F. Yang, Y. Gao, C. Xu and L. Wang, *Sci. Adv.*, 2020, **6**, eaaz8204.

22 J. Wang, W. Jin, S. Huang, W. Wang, S. Wang, Z. Yu, L. Gao, Y. Gao, H. Han and L. Wang, *Angew. Chem., Int. Ed.*, 2024, **63**, e202314583.

23 W. J. Yang, X. Wang, R. Zhang, Y. Wang, Q. Qiu, L. Yuwen and L. Wang, *J. Mater. Chem. B*, 2021, **9**, 2266–2274.

24 Z. Yang and H. Chen, *View*, 2022, **3**, 20220009.

25 J. Yin, S. Wang, J. Wang, Y. Zhang, C. Fan, J. Chao, Y. Gao and L. Wang, *Nat. Mater.*, 2024, 1–9, DOI: **10.1038/s41563-024-01826-y**.

26 P. Lavrador, M. R. Esteves, V. M. Gaspar and J. F. Mano, *Adv. Funct. Mater.*, 2020, **31**, 2005941.

27 W. Xu, W. Wang, S. Chen, R. Zhang, Y. Wang, Q. Zhang, L. Yuwen, W. J. Yang and L. Wang, *J. Colloid Interface Sci.*, 2021, **586**, 601–612.

28 Y. Zhang, W. Xiu, Y. Sun, D. Zhu, Q. Zhang, L. Yuwen, L. Weng, Z. Teng and L. Wang, *Nanoscale*, 2017, **9**, 15835–15845.

29 Y. Zhang and C. Jiang, *J. Controlled Release*, 2021, **330**, 554–564.

30 H. Ren, Z. Zhang, X. Cheng, Z. Zou, X. Chen and C. He, *Sci. Adv.*, 2023, **9**, eadh4327.

31 L. Huang, Y. Li, Y. Du, Y. Zhang, X. Wang, Y. Ding, X. Yang, F. Meng, J. Tu, L. Luo and C. Sun, *Nat. Commun.*, 2019, **10**, 4871.

32 M. Chen, H. Li, J. Zang, Y. Deng, H. Li, Q. Wu, T. Ci and Z. Gu, *Biomaterials*, 2023, **302**, 122319.

33 Q. Li, M. Dang, J. Tao, X. Li, W. Xiu, Z. Dai, A. He, M. Ding, Y. Zhang, Z. F. Wen, X. Su, A. J. Elbourne, L. Bao, L. Chen, Y. Mou, Z. Teng and H. Dong, *Adv. Funct. Mater.*, 2024, 2311480.

34 Y. Zhang, Q. Li, M. Ding, W. Xiu, J. Shan, L. Yuwen, D. Yang, X. Song, G. Yang, X. Su, Y. Mou, Z. Teng and H. Dong, *Adv. Healthc. Mater.*, 2023, **12**, e2203028.

35 L. Chen, X. Lin, S. Shi, M. Li, M. Mortimer, W. Fang, F. Li and L. H. Guo, *Sci. Total Environ.*, 2023, **901**, 166257.

This journal is © The Royal Society of Chemistry 2024